Atmos. Chem. Phys. Discuss., 14, 20117–20157, 2014
www.atmos-chem-phys-discuss.net/14/20117/2014/
doi:10.5194/acpd-14-20117-2014

Atmospheric Chemistry and Physics Discussions

A high ozone episode in winter 2013 in the Uinta Basin oil and gas region characterized by aircraft measurements

S. J. Oltmans[1,2], A. Karion[1,2], R. C. Schnell[2], G. Pétron[1,2], C. Sweeney[1,2], S. Wolter[1,2], D. Neff[1,2], S. A. Montzka[2], B. R. Miller[1,2], D. Helmig[3], B. J. Johnson[2], and J. Hueber[3]

[1]CIRES, University of Colorado, Boulder, Colorado, USA
[2]NOAA/ESRL, Global Monitoring Division, Boulder, Colorado, USA
[3]INSTAAR, University of Colorado, Boulder, Colorado, USA

Received: 19 June 2014 – Accepted: 6 July 2014 – Published: 4 August 2014

Correspondence to: S. J. Oltmans (samuel.j.oltmans@noaa.gov)

Published by Copernicus Publications on behalf of the European Geosciences Union.

Abstract

During the winter of 2012–2013 atmospheric surface ozone mole fractions exceeded the US 8 h standard of 75 ppb on 39 days in the Uinta Basin of Utah. As part of the Uinta Basin Winter Ozone Study (UBWOS) aircraft flights were conducted throughout the basin with continuous measurements of ozone (O_3), methane (CH_4), carbon dioxide (CO_2), carbon monoxide (CO), nitrogen dioxide (NO_2), and discrete whole air flask samples for determination of ~ 50 trace gases including a number of non-methane hydrocarbons (NMHCs). During the course of seven flights conducted between 31 January and 7 February 2013, coinciding with strong, multi-day temperature inversions, O_3 levels gradually built up in the shallow boundary layer from ~ 45 ppb to ~ 140 ppb. Near-surface CH_4 mole fractions increased during the episode from near background levels of ~ 2 ppm to over 10 ppm. Based on elevated levels of CH_4 across the basin and high correlations of CH_4 with NMHCs from the discrete air samples, O_3 precursor NMHCs were also inferred to be elevated throughout the basin. Discrete plumes of high NO_2 were observed in the gas production region of the basin suggesting that gas processing plants and compressor facilities were important point sources of reactive nitrogen oxides (NO_x). Vertical profiles obtained during the flights showed that the high O_3 mole fractions (as well as other elevated constituents) were confined to a shallow layer from near the ground to 300–400 m above ground level (m a.g.l.) capped by a strong temperature inversion. The highest mole fractions of the measured constituents during the study period were in an isothermal cold layer that varied from ~ 300 m depth on 4 February to ~ 150 m on 5 February. A gradient layer with declining mole fractions with altitude extended above the isothermal layer to ~ 1900 m a.s.l. (300–400 m a.g.l.) indicative of some mixing of air out of the boundary layer. O_3 mole fractions continued to increase within the basin as the high O_3 episode developed over the course of a week. CH_4 mole fractions, on the other hand, leveled off after several days. On several flights, the aircraft sampled the plume of a coal-fired power plant (located east of the main gas field) flowing above the inversion layer. These measurements ruled out the effluents of

ACPD
14, 20117–20157, 2014

the power plant as a significant source of NO_x for O_3 production beneath the temperature inversion in the basin. The presence of elevated O_3 precursors within the basin and the rapid daytime production of O_3 in the atmosphere beneath the temperature inversion both indicated that O_3 was being produced from precursors emitted within the basin beneath the temperature inversion. Although observations show that horizontal winds in the surface layer were relatively light during the high ozone event, they were sufficient to disperse precursors up to 80 km from primary sources in the main gas field in the southeast quadrant to the balance of the Uinta Basin.

1 Introduction

While vigorous ozone formation in the summer under conditions with high levels of solar insolation and abundant O_3 precursor concentrations has long been recognized (Chameides et al., 1992), high levels of O_3 production during the winter has only recently been documented in two oil and gas basins in the Rocky Mountain US (Schnell et al., 2009; Oltmans et al., 2014; Rappenglueck et al., 2014). In these two basins, the strong role of meteorology, topography, and high levels of O_3 precursors from oil and gas extraction activities have been identified as key drivers of wintertime high O_3 events. The presence of snow-covered terrain acts as both an enhancer of available ultraviolet (UV) radiation by greatly increasing the surface albedo, and promoter of strong temperature inversions that trap O_3 precursor emissions in a shallow surface layer (Yu and Pielke, 1986; Oltmans et al., 2014). A geographic basin such as the Uinta surrounded by elevated terrain inhibits the flushing of air trapped below the inversion (Bader and McKee, 1985). Emissions from oil and gas production and processing activities as well as combustion emissions associated with vehicle traffic, drilling rigs, compressor stations and gas processing may be significant sources of both volatile organic compounds (VOCs) (Gilman et al., 2013; Warneke et al., 2014) and nitrogen oxides ($NO_x = NO + NO_2$), primary O_3 precursors. As part of the 2013 Uinta Basin Winter Ozone Study (UBWOS) campaign aircraft flights were carried out in the context of

ACPD
14, 20117–20157, 2014

extensive field measurements (Stoeckenius and McNally, 2014). These measurements included ozone profiles from tethered ozonesondes (Schnell et al., 2014) at three sites in the basin. Wind speed and direction profiles (Stoeckenius and McNally, 2014), hydrocarbon and nitrogen oxide mole fraction profiles (Helmig et al., 2014), an intensive set of chemical constituent observations (Stoeckenius and McNally, 2014), and meteorological variables (Stoeckenius and McNally, 2014) were also obtained for 6 weeks at the Horse Pool fixed site on the northern edge of the gas field south of Vernal, Utah. In addition, a number of surface observing sites were operated throughout the basin measuring O_3, NO_x, and meteorological parameters (Stoeckenius and McNally, 2014). During the period December 2012–March 2013 conditions favorable for strong ozone formation were present associated with continuous snow cover that produced strong, shallow, stable boundary layers capped by strong temperature inversions and high surface albedos (Oltmans et al., 2014; Stoeckenius and McNally, 2014)

The UBWOS 2013 study took place in the Uinta Basin located in NE Utah (Fig. 1). The basin is characterized by tight oil and gas formations requiring techniques such as hydraulic fracturing to access deposits. Natural gas production is found mainly on the east side of the basin in Uintah County (88 %) and oil primarily on the west side in Duchesne County (70 %). In 2013 there were ~ 6000 natural gas wells and ~ 4000 oil wells in operation. Drilling commenced on ~ 80 wells (spudded wells) each month during January–March 2013. During January–March 2013 the combined annualized oil production (4x the seasonal production for comparison with the full year production) for the two counties was ~ 28 million barrels per year and the gas production was ~ 3.5 trillion cubic feet per year. This is about 2 million barrels per year more than the average oil production and 0.2 trillion cubic feet per year less than the average gas production for the full years of 2012 and 2013 (source: Utah Oil and Gas Program – http://oilgas.ogm.utah.gov/). The population of Duchesne and Uintah counties is ~ 55 000 residents with the towns of Vernal and Roosevelt being the largest population centers. These two communities and the highway bisecting the basin east to west are likely sources

ACPD
14, 20117–20157, 2014

of transportation related emissions, particularly of NO_x, outside of oil and gas related activities.

High wintertime O_3 readings were first reported in the Uinta Basin in 2009–2010 (Martin et al., 2011; Oltmans et al., 2014). The UBWOS in 2012 and 2013 were initiated to investigate the drivers of high wintertime O_3 (Lyman and Shorthill, 2013; Stoeckenius and McNally, 2014). In February 2012 and February 2013 aircraft measurements provided a unique view of basin-wide atmospheric constituent concentrations. During the 2012–2013 winter with a number of episodes of persistent high O_3 mole fraction at the surface (Oltmans et al., 2014), O_3 and a number of trace gases emitted by O_3 precursor sources were measured to document their spatial distribution across the basin and vertically from near the surface to above the strong capping temperature inversion. In addition, correlations between the measured constituents were determined separately for four spatial quadrants within the basin. Over the course of a week, daily aircraft flights tracked the evolution of a high O_3 episode from its initiation at near background conditions to its peak. The exhaust plume from a coal-fired power plant located within the basin was also measured to determine its role as a potential source of O_3 precursors contributing to O_3 formation within the basin.

2 Methodologies

During the UBWOS 2013 campaign, a single-engine Cessna 210 aircraft (owned and operated by Kalscott Engineering, www.kalscott.com) was deployed in the Uinta Basin by the NOAA Global Monitoring Division's (GMD) aircraft program (Fig. 2). Instruments drew air through dedicated inlets installed under the aircraft's starboard wing (Fig. 2). On-board instrumentation included high-frequency analyzers for carbon monoxide (CO), carbon dioxide (CO_2), methane (CH_4), and water vapor (H_2O) (Picarro G2401m), nitrogen dioxide (NO_2) (Los Gatos Research Model 911-0009), and ozone (O_3) (2B Systems Model 211). NOAA GMD custom flask packages were used to collect discrete air samples that were sent back to NOAA GMD in Boulder for analysis

ACPD
14, 20117–20157, 2014

of 50+ trace gases, including CO, CO_2, CH_4, and light hydrocarbons such as C_3H_8 (propane), C_4H_{10} (butane), C_5H_{12} (pentane), C_2H_2 (acetylene), C_6H_6 (benzene) (Karion et al., 2013a, http://www.esrl.noaa.gov/gmd/ccgg/aircraft/analysis.html). The same air samples were then analyzed for additional hydrocarbons, including ethane, hexane isomers, and toluene at the University of Colorado Institute of Arctic and Alpine Research (INSTAAR) (Helmig et al., 2009, 2014). GPS location information, temperature, relative humidity, and ambient pressure measurements were also collected onboard and synchronized with the ambient gas measurements. Measurements of trace gases both from the in-situ continuous analyzers (except for O_3 and NO_2) and the flask packages are all reported on the NOAA/WMO scales as dry air mole fractions (moles per mole of dry air), using methods outlined in Karion et al. (2013a) and online at http://www.esrl.noaa.gov/gmd/ccgg/aircraft/analysis.html. Measurements of O_3 were made with a fast-response version of the 2B Technologies, Boulder, CO UV photometric analyzer which used nitric oxide (NO) in place of a solid phase scrubber to avoid potential inference from aromatics and mercury. This instrument was calibrated before and after the campaign against a NOAA GMD maintained standard that is regularly compared with a US NIST standard. Measurements of NO_2 have an internal instrument "zero cycle" calibration. The NO_2 instrument was factory calibrated prior to the field deployment. O_3 and NO_2 are expressed as mole fractions, which are equivalent to mixing ratios when referred to ambient air (as opposed to dry air).

Seven research flights were conducted over an 8 day period from 31 January to 7 February 2013. During this period snow-covered ground, low surface temperatures, low wind speeds, lack of cloud cover, and emission confining topography all provided excellent conditions for highly stratified temperature, inversion capped near-surface conditions where emissions and secondary products were trapped. Surface temperatures regularly dipped below −10 °C during the study period. Research flights surveyed the region, generally flying within the inversion capped surface layer or dipping in and out of the near surface layer.

ACPD
14, 20117–20157, 2014

3 Results

Flights were conducted during a multi-day episode of ozone pollution at the surface to characterize spatial and temporal features of the constituents measured on the aircraft. During the 8 day period over which the aircraft flights were conducted, surface ozone hourly mole fractions built up from approximately background levels of 45 ppb to over 140 ppb (Fig. 3). The first flight on 31 January occurred after the basin had been flushed out by the passage of a frontal system three days earlier. The final flight on 7 February took place just prior to the passage of another weather disturbance that again led to the flushing of ozone and related gases measured by the aircraft out of the basin, bringing concentrations back to near background levels.

3.1 Spatial distribution of O_3, CH_4, CO, CO_2, and NO_2

The spatial distributions of O_3, CH_4, CO, CO_2, and NO_2 within the surface layer were mapped out over the basin during the campaign. Although the flight tracks did not cover all portions of the basin on each flight day, a rich body of information on the evolving distribution of constituents in the basin was obtained. Figure 4 shows the distribution of O_3 measured over the Uinta Basin on 31 January, 1, 2, 4, 5, and 6 February. The flight tracks show data collected below 1650 m above sea level (m a.s.l.). There was a continuing buildup of O_3 through the progression of flights. On 31 January, O_3 mole fractions over most of the basin were less than $\sim$ 60 ppb with values near 80 ppb in the SE sector near the primary gas field. By 1 February, O_3 was already > 80 ppb over large portions of the basin and the high values were not confined to the SE. This pattern continued as ozone built up throughout the course of the week reaching values in excess of 140 ppb. The flights on 1 and 2 February had the most extensive coverage of the basin below 1650 m a.s.l. and very clearly showed that high O_3 was ubiquitous throughout the inversion capped surface layer in the basin not just in the vicinity of the gas field.

ACPD
14, 20117–20157, 2014

On 31 January, two days after the basin had been swept out by the passage of a cold front CH_4 values over most of the basin were generally below 3 ppm except near the gas field (Fig. 5). However, by 1 February CH_4 mole fractions of 5 ppm were widespread over the basin. After 2 February, CH_4 mole fractions were > 6 ppm over much of the basin with much higher values (> 8 ppm) over the gas field and immediately to the west. Of particular note were the extremely high values (> 10 ppm) in the vicinity of the primary gas field. Unlike O_3, CH_4 did not exhibit a continuous buildup through the entire period appearing to plateau after 4 February. The lack of buildup after 4 February, suggests that later in the episode air was partially mixed out of the boundary layer. This is investigated in a later section discussing the vertical profile observations. The leveling off of CH_4 is consistent with the surface CH_4 measurements made at the Horse Pool site (Helmig et al., 2014). As shown in a later section discussing the discrete flask samples, the high CH_4 values reflect strong emissions from oil and gas operations leading to very high atmospheric non-methane hydrocarbon (NMHC) atmospheric mole fractions across the entire basin during inversion episodes.

CO with a relatively long lifetime (> 2 months) is indicative of combustion sources. NO_2 has a relatively short lifetime as a result of reactions with NO mediated by high O_3 mole fractions. The spatial patterns for CO and NO_2 are shown in Fig. 6 for 2 February. CO values were moderately elevated above the gas field (200–300 ppb) but the highest values of CO (> 600 ppb) measured during the flights were in the SW sector over the region of oil production in Duchesne County. No other constituents measured in this sector showed values elevated above those seen in other parts of the basin. Neither high CO_2 nor NO_2 values accompanied these high CO mole fractions measured over the oil fields

NO_2 mole fractions were very high (> 10 ppb) over large portions of the gas field while only occasional local elevated values (> 4 ppb) were measured over the rest of the basin. Although the flight tracks within the near surface layer on days other than 2 February did not cover the basin as systematically, the patterns for CO and NO_2 replicate the basic patterns seen on 2 February.

ACPD
14, 20117–20157, 2014

3.2 Relationships between chemical constituents in the basin

To analyze the trace gas enhancements and their relationships across the different regions of the basin, the flight tracks were separated into four spatial quadrants: South-East (SE), South-West (SW), North-East (NE), and North-West (NW). Trace gas observations from each quadrant are colored differently (Fig. 7a) and correlations between the different measured species for altitudes below 1650 m a.s.l. are investigated (Fig. 7b–d). An analysis of the measurements collected on 2 February shows elevated CO (up to 700 ppb) in the SW quadrant relative to all the other species and relative to the other quadrants. In the SE, CH_4 was enhanced more per unit CO than in the SW, while in the SW, more CO was present per unit CH_4 (Fig. 7c). In the SW, more CO was generated per unit CO_2 as well, indicating the presence of an inefficient combustion source in that area. The enhancement ratio of CO to CO_2 in the SW (green in Fig. 7b) was significantly greater than those reported in the literature for either direct tailpipe vehicular emissions (9–18 ppb CO $(\text{ppm } CO_2)^{-1}$ (Bishop and Stedman, 2008)) or urban areas (10–14 ppb CO $(\text{ppm } CO_2)^{-1}$), (Wunch et al., 2009; Turnbull et al., 2011; Miller et al., 2012; Peischl et al., 2013) shown by the black lines in Fig. 7b). The relatively larger enhancements of CO in the SW quadrant and enhancements of CH_4 in the SE were present in all flights. The correlations plots for the emitted species that were measured with the aircraft; CO to CH_4 (Fig. 8), CO to NO_2 (Fig. 9), and CH_4 to NO_2 (Fig. 10) are shown for all seven flights in 2013.

On most days, CH_4 mole fractions were lower in the NW and SW quadrants than in the SE, an indication that the gas field in the southern part of Uintah County has higher CH_4 emissions than the oil field on the western side of the basin. This was also observed in flights conducted over the same region the previous year, in February 2012 (Lyman and Shorthill, 2013; Karion et al., 2013b), indicating that a significant portion of CH_4 emissions in this quadrant were persistent. Possible CH_4 emissions sources in the SE quadrant include a dense array of compressor stations and two large processing

ACPD
14, 20117–20157, 2014

plants (the Chipeta Plant Complex and Stagecoach/QEP). Quantitative estimates of contributions from these various O_3 precursor sources are still unknown.

Although NO_x ($NO+NO_2$) are mainly emitted from combustion sources (just as CO is), the most elevated NO_2 was not observed in the same region as the elevated CO (Fig. 9). In the flight data, NO_2 mole fractions were highest in the same SE region as the elevated CH_4, although they were not well correlated with CH_4 (Fig. 10), which indicates there were CH_4 point sources that have no NO_2 emissions and vice versa. Based on the flight data, it appears that release of NO_2 was occurring preferentially near the processing plants and compressor stations in the SE quadrant.

Figure 11 (panels 1–5) shows the measurements of light NMHC species that are components of raw natural gas as they correlate with CH_4 in air samples collected in flasks aboard the aircraft. The data for 2013 are shown by quadrant with the colors designating the same sectors as in Fig. 7. For 2012 samples are shown as light gray symbols; this comparison emphasizes the higher values in 2013. Mole fractions of propane (C_3H_8), *n*-butane (*n*-C_4H_{10}), *n*-pentane (*n*-C_5H_{12}), iso-pentane (*i*-C_5H_{12}), and benzene (C_6H_6) show high correlation with CH_4 in both years. Given the high correlations between the NMHCs and CH_4 in the aircraft air samples in winters 2011–2012 and 2012–2013 the inference is that these NMHCs are likely distributed across the basin similarly to CH_4 since they are co-emitted with CH_4 when natural gas is leaked into the atmosphere. Figure 11 (bottom right panel) also shows the relationship between CO and CH_4 measured in flask samples in each year. These gases are less well correlated, as discussed in the previous section for the continuous data, with the SW sector having higher CO relative to CH_4. The similar relationship between CH_4 and CO seen in the flasks compared to the continuous measurements provides evidence that the more limited flask samples are representative of conditions in the basin. Figure 12 shows winter 2012–2013 measurements of heavier hydrocarbons in the same flasks which are all strongly correlated with CH_4 and significantly enhanced. This correlation is indicative of the availability of O_3 precursor NMHCs along with CH_4 emissions. All species were present in significantly higher concentrations in winter 2012–2013

ACPD
14, 20117–20157, 2014

compared with 2011–2012. In winter 2011–2012, boundary layer heights were between 500 and 1000 m a.g.l. during the campaign, while in winter 2012–2013 the emissions were contained within a layer of only 100–300 m as may be observed in the vertical profile measurements discussed later.

3.3 Relationship of O_3 to other constituents measured on the aircraft

CH_4 values were highest near the gas fields in the SE sector but high CH_4 values (Fig. 5) and high coincident NMHC mole fractions in discrete air samples were seen across the basin (Figs. 11 and 12). Also, O_3 mole fractions were high throughout the near-surface layer in the Uinta Basin (Fig. 4).

In general, O_3 increases with increasing CH_4 (Fig. 13) although for the very highest CH_4 values (> 8 ppm), seen primarily in the SE sector where the primary gas field is located, this is not the case, especially when peak O_3 values are < 100 ppb (Fig. 13). The relationship between O_3 and CH_4 appears similar throughout the basin with the exception of the very high CH_4 in the SE.

Figure 14 shows a general O_3 increase with increasing CO. The most anomalous feature is the very large CO values in the SW sector that do not correlate with O_3. These much higher CO values in the SW are apparent in the relationship with all the trace gases measured on the aircraft including CH_4, CO_2, and NO_2 (see Figs. 7–10).

As can be see seen in Fig. 14, O_3 and NO_2 are not well correlated. While occasional values of NO_2 > 5 ppb are seen in all of the sectors, this level is regularly seen and often exceeded (NO_2 > 10 ppb) in the SE sector (red points) indicating that this is an area of large NO_x emissions.

3.4 Vertical distribution of O_3 and other constituents

During each of the seven aircraft flights in 2013, the aircraft conducted two or more vertical profiles, in which measurements were collected either in a spiral ascent or descent, or during an ascent/descent that also transited horizontally. Data collected

ACPD
14, 20117–20157, 2014

during these profiles are valuable in assessing the extent of vertical mixing within the inversion layer, quantifying the gradient in mole fractions of species above and within the inversion layer, and observing features that exist above the inversion layer. The sharp vertical gradient in the measured constituents associated with the persistent temperature inversion are captured in profile measurements at a number of locations within the basin. A set of four profiles early in the episode (31 January–2 February) (Fig. 16) presents a picture of the early buildup and variation across the basin. The profile on 31 January (profile 1/31) located to the south of the oil field shows only a slight enhancement of the measured constituents including O_3 below the inversion. Above the inversion to near the top of the aircraft profile all of the constituents show constant values near the regional tropospheric background levels. Two profiles on 1 February illustrate conditions over the gas field and appreciably away from the gas field. Near the gas field below ~ 1600 m a.s.l. (~ 150 m a.g.l.) CH_4 was > 10 ppm, NO_2 > 10 ppb, and CO and CO_2 were also enhanced. O_3 was modestly enhanced to ~ 60 ppb compared to the layer above. All the constituents showed a strong gradient with values declining markedly between the lowest altitude and the top of the cold layer defined by the nearly constant temperatures < −5 °C. Above this layer the concentrations declined further to near background values at ~ 1700 m a.s.l.. The second profile on 1 February was obtained in the northwest quadrant away from the gas field. At this location there was a weaker temperature inversion with a top at ~ 1700 m a.s.l.. All of the constituents were enhanced with O_3 much higher (~ 80 ppb) than near the gas field. There was also a weaker gradient with all the constituents enhanced up to 2000 m compared to the near-background levels seen in the upper portion of the profile over the gas field. The profile on 2 February was above the Horse Pool surface site. A relatively shallow cold layer defined by the nearly constant temperatures < −5 °C from the surface to ~ 1600 m a.s.l. was overlain by a more vertically structured layer up to the level where the strong temperature increase (~ 5° C) ended at ~ 1750 m. O_3 mole fractions of ~ 90 ppb reflect an increase from the previous day.

ACPD
14, 20117–20157, 2014

A set of six profiles on 4 February (Fig. 17) provides a picture of the profile structure at various locations in the basin covering a period from early to late afternoon (Fig. 17a). In all of these profiles O_3 in the layer below 1700–1750 m a.s.l. was > 80 ppb. All of the other aircraft measured constituents also showed significant enhancements. By 5 February (Fig. 18) O_3 at all four profile locations was > 100 ppb in the layer below 1600 m a.s.l. where there was a distinct change in the temperature gradient with warmer air aloft. The layer with the largest constituent mole fractions was 100 m shallower than on the previous day consistent with the lower altitude of the strongest temperature gradient on 5 February. Between altitudes 1600–1900 m a.s.l. there was a gradual decrease in all of the constituents but the mole fractions were somewhat elevated above the tropospheric background up to ~ 2400 m a.s.l.

A number of profiles in relatively close proximity to the Bonanza power plant encountered a layer downwind of the plant at an altitude of 1900–2000 m a.s.l. containing enhanced CO, CO_2 and NO_2 but with no enhancement in CH_4 and depleted O_3. Notably, the depression of O_3 mole fractions below the O_3 measured outside the plume was a clear indication of O_3 titration by the power plant emitted NO. On 4 February this plume was located near the top or just above the cold pool layer at ~ 1800 m a.s.l. On 5 February the plume was a bit higher at ~ 1900 m a.s.l. The buoyant plume of emissions from the power plant, whose stack height is at 192 m a.g.l., or 1815 m a.s.l., appeared to be lofted above the stack height as seen in Fig. 19 but then settled somewhat as the plume cooled. The plume was then stabilized above the top of the temperature capped inversion layer, and remained above the inversion in a plume that varied in altitude between 1800–1900 m a.s.l. The combustion products observed in the plume (CO, CO_2, and NO_2) all declined immediately below the plume before rising again at lower altitudes, evidence that the plume was not mixing to lower altitudes and was not contributing to precursors near the surface where O_3 was formed. The sharp boundary of the bottom of the plume also provided a marker for the top of the layer influenced by the surface emissions and O_3 production.

ACPD
14, 20117–20157, 2014

4 Discussion and conclusions

Extensive airborne measurements (including vertical profiles) across the Uinta Basin over a one week span encompassing a major ozone episode, gives a unique and comprehensive picture of emissions from oil and gas production activities and their role in wintertime O_3 formation in the Uinta Basin. While the largest CH_4 mole fractions were found near the primary gas field in the eastern portion of the basin, high CH_4, mole fractions > 5 ppm were seen in all four quadrants of the basin (Fig. 5). There is a strong relationship between CH_4 and the suite of NMHCs obtained from the flask samples (Fig. 12) that was consistent across all four quadrants of the basin. The implication is that these compounds were not only emitted together, but also dispersed together across the basin. Even in the northeast and northwest quadrants, where there are few oil and gas wells, CH_4 (> 5 ppm) and NMHCs can be significantly elevated. Although wind measurements were not made on the airplane, the tethered ozonesonde measurements at Ouray and Fantasy Canyon (Schnell et al., 2014) provided useful wind direction information with height throughout the day for the period of the aircraft flights (an example for two days is shown in Fig. 20). In the height interval from near the surface to top of the inversion layer wind direction consistently had an easterly component (winds from the east). This flow feature was also found during daytime hours in the modeling performed by Neemann et al. (2014). This provides evidence that the high CH_4 (and strongly correlated NMHC) mole fractions seen across the basin were a result of air movement across the basin from the gas field.

The largest concentrations of NO_2 were seen in the SE quadrant (Fig. 6) where CH_4 was also highest. While both of these constituents were high in this sector they are not well correlated (Fig. 10) suggesting separate point sources. In the SE sector there is a tendency for NO_2 and CO to be better correlated (Fig. 9) suggesting a common combustion related source for both. In other quadrants there is not a consistent relationship. A notable feature of CO was the very high concentrations in the SW quadrant in comparison to all other sectors (Figs. 6, 7, 8, and 9). Beginning on 1 February when the

ACPD
14, 20117–20157, 2014

temperature inversion over the basin became well-established CO values > 600 ppb were seen every day in the SW. Based on the relationship with CO_2 (Fig. 7) these high CO mole fractions suggest an inefficient combustion source. Since this quadrant encompasses the main oil field a potential source for the high CO was inefficient pump jack engine operation.

The general increases of O_3 mole fractions with increasing CH_4 and CO except at the very highest values (CH_4 > 8 ppm, CO > 400 ppb) in all sectors of the basin on each flight day (Figs. 13 and 14) are strong indicators of the link between CH_4 and CO and the O_3 precursors responsible for vigorous O_3 production. The primary source of elevated CO mole fractions in the basin is combustion based on the relationship between CO and CO_2 with O_3 precursor NO_x as a known additional emitted product of combustion. Because of the chemical interchange between NO and NO_2 in the production of O_3 the relationship between O_3 and NO_2 in the aircraft measurements is not straightforward (Fig. 15). However, large mole fractions of NO_2 (> 5 ppb) were seen throughout the basin with especially large mole fractions in the SE quadrant signaling the availability of NO_x as well as precursor NMHCs for very active O_3 photochemistry.

O_3 mole fractions increased across the basin during the course of the ozone episode (Figs. 3 and 4) while CH_4 values increased over the first four days but did not appear to continue to rise along with O_3 through the remainder of the flight period (Figs. 5 and 13). On the assumption that CH_4 emissions remain relatively constant, transport out of the boundary layer appears to limit the increase in CH_4 during the latter days of elevated ozone event. This is suggested by the profiles of 4 and 5 February (Figs. 18 and 19) where there is a falloff in mole fractions of CH_4 in the gradient region between the top of the near constant cold layer and the level where tropospheric background levels were reached at 1900–2000 m, indicative of a weaker capping of air above the cold layer. O_3 mole fractions continued to increase across the basin through the flight period (also seen in surface measurements and tether ozonesonde profiles – Fig. 3 and Schnell et al., 2014) although they also showed the drop off in the gradient layer on 4 and 5 February seen in CH_4 and CO and CO_2. Unlike CH_4, O_3 levels were strongly

ACPD
14, 20117–20157, 2014

influenced by chemical production and loss processes over the time interval of the aircraft flights. During the course of the O_3 event daily minimum values, seen during the night, continued to rise (Fig. 3) (Schnell et al., 2014) indicating that chemical loss, surface deposition, and transport out of the boundary layer did not fully remove O_3 from the previous day's production. Although CH_4 (and likely also accompanying NMHC) levels stabilize after a few days, they remained sufficiently high to fuel O_3 production and increasing O_3 mole fractions throughout the event captured by the aircraft flights.

The persistent snow cover in the Uinta Basin through the winter of 2012–2013 led to extended periods with well-developed temperature inversions resulting in a stable near surface layer. Although the entire period of the aircraft flights was characterized by a stable surface layer (Figs. 16, 17, and 18) significant variation was seen in this layer both in the temperature structure and the distribution of the gas constituents within the layer. In the early flights (Fig. 16) the temperature gradient was weaker with the near surface inversion at 1600–1700 m a.s.l. and the strongest enhancements of the measured gas constituents below the temperature inversion. However, some enhancement was seen above the inversion especially in a profile on 1 February (Profile 2/1 in Fig. 16) when only a very weak inversion was present indicating at least some venting from the boundary layer even early in the high O_3 episode. On 4 February the cold (isothermal) layer was deeper with the top at ~ 1750 m a.s.l. in all of the profiles (Fig. 17) and the strongest enhancement in O_3 and the other measured constituents was found within this layer. The decline to near tropospheric background mole fractions occurred within a relatively narrow layer of ~ 150 m. This deeper, isothermal temperature layer up to1700–1800 m a.s.l., may have been partially responsible for the lower (though still high) peak surface O_3 seen on 4 February than on the previous day and following day (Fig. 3). CH_4 and O_3 have near-constant mole fractions through this thicker layer. On 5 February there is a much shallower cold isothermal layer with a sharp change in temperature gradient at ~ 1600 m a.s.l. This layer has very high mole fractions of all of the other measured constituents, including O_3. A consistent feature of the profiles throughout the aircraft flights was an isothermal layer near the surface in the coldest portion of

ACPD
14, 20117–20157, 2014

the profile beneath the temperature inversion. As noted above, this layer was of varying depths but as on 5 February could encompass a large portion of the layer below the inversion. Within this layer all of the constituents had near-constant mole fractions consistent with some level of mixing within the layer. Since the aircraft flights were conducted between late morning and late afternoon during sunlit hours, the suggestion is that heating of the surface was sufficient to produce mixing within the layer represented by the resultant isothermal temperatures. The gradient layer that extended above the shallow isothermal cold layer also contained large but decreasing O_3 mole fractions. The presence of a gradient from the layer with the highest constituent fractions near the surface to ~ 2000 m a.s.l. is indicative of mixing out of the boundary layer even as O_3 is building up. With the exception of the power plant plume that resided just at the top of the inversion layer the aircraft profiles showed increasing constituent mole fractions below the inversion with the lowest mole fractions above the inversion. This was a strong indication that the source of high constituent mole fractions was from within the basin and that the source was not located outside of the basin, including urban Salt Lake City.

Continuous measurements of O_3, CH_4, CO, CO_2, and NO_2 along with periodic flask measurements during the seven aircraft flights between 31 January and 7 February 2013 link the enhanced O_3 production during the winter of 2012–2013 with precursor emission sources primarily in the vicinity of the main gas field. The high O_3 mole fractions seen over the entire basin well away from large precursor sources suggest widespread dispersal of the precursors and O_3 production across the basin. The strongest O_3 enhancements were seen in a relatively shallow surface layer with a strong temperature inversion with a top near 1700 ± 50 m a.s.l. There was a gradient layer above this inversion with elevated constituent mole fractions that gradually declined to near tropospheric background values between 1900–2000 m a.s.l. This gradient layer was indicative of limited mixing of air out of the surface layer even as emissions and O_3 were continuing to build up. Constituents such as CH_4 that were not subject to chemical formation stabilized after ~ 4 days from the beginning of an

ACPD
14, 20117–20157, 2014

O_3 event while continued O_3 production led to increasing O_3 through the episode. The meteorological conditions seen in the Uinta Basin during winter 2013 promoted the formation of a shallow inversion layer due to persistent snow cover and relatively long periods (approximately one week) without basin flushing frontal passages. Based on precursor emission levels and meteorological conditions similar to those seen in 2013 in the Uinta Basin, it is likely that high O_3 episodes can be expected in the future. Modeling of the conditions in winter in 2011–2012 and 2012–2013 (Edwards et al., 2013; Neemann et al., 2014; Ahmadov et al., 2014) also show the vital role of snow cover that promotes and sustains strong temperature inversions, enhanced UV from high albedos, and reduced O_3 deposition in combination with highly elevated levels of O_3 precursors.

Acknowledgements. Funding for the aircraft flights was provided by the NOAA Climate Program Office. The NO_2 analyzer used on the aircraft was generously loaned to NOAA/GMD by Russ Dickerson of the University of Maryland. Partial funding for the purchase of the NO_2 analyzer was provided through Russ Dickerson's participation in the NASA AQAST program. The skilled piloting of the aircraft by C. Midyett was a key element in obtaining the extensive data set used in this study.

The 2013 Uinta Basin Ozone Study was funded by and provided in-kind support by the: Uintah Impact Mitigation Special Service District (UIMSSD), Western Energy Alliance, QEP Resources, Inc., Bureau of Land Management (BLM), National Oceanic and Atmospheric Administration (NOAA), Environmental Protection Agency (EPA), Utah Department of Environmental Quality (UDEQ) and Utah Science Technology and Research Initiative (USTAR), and Utah School and Institutional Trust Lands Administration (SITLA).

References

Ahmadov, R., McKeen, S., Trainer, M., Banta, R., Brewer, A., Brown, S., Edwards, P., de Gouw, J., Frost, G. J., Gilman, J. Helmig, D., Johnson, B., Karion, A., Koss, A., Langford, A., Lerner, B., Olson, J., Oltmans, S., Parrish, D., Peischl, J., Petron, G., Pichugina, Y., Roberts, J. M., Ryerson, T., Schnell, R., Senff, C., Sweeney, C., Veres, P., Warneke, C.,

ACPD
14, 20117–20157, 2014

Wild, R., Williams, E. J., Zamora, R.: Understanding high wintertime ozone in oil and natural gas producing region of the western US, Atmos. Chem. Phys. Discuss., in press, 2014.
Bader, D. C. and McKee, T. B.: Effects of shear, stability and valley characteristics on the destruction of temperature inversions, J. Clim. Appl. Meteorol., 24, 822–832, 1985.
Bishop, G. A. and Stedman, D. H.: A decade of on-road emissions measurements, Environ. Sci. Technol., 42, 1651–1656, 2008.
Chameides, W. L., Fehsenfeld, F., Rodgers, M. O., Cardelino, C., Martinez, J., Parrish, D, Lonneman, W., Lawson, D. R., Rasmussen, R. A., Zimmerman, P., Greenberg, J., Middleton, P., and Wang, T.: Ozone precursor relationships in the ambient atmosphere, J. Geophys. Res.-Atmos., 1992, 97, 6037–6055, 1992.
Edwards, P. M., Young, C. J., Aikin, K., deGouw, J., Dubé, W. P., Geiger, F., Gilman, J., Helmig, D., Holloway, J. S., Kercher, J., Lerner, B., Martin, R., McLaren, R., Parrish, D. D., Peischl, J., Roberts, J. M., Ryerson, T. B., Thornton, J., Warneke, C., Williams, E. J., and Brown, S. S.: Ozone photochemistry in an oil and natural gas extraction region during winter: simulations of a snow-free season in the Uintah Basin, Utah, Atmos. Chem. Phys., 13, 8955–8971, doi:10.5194/acp-13-8955-2013, 2013.
Gilman, J. B., Lerner, B. M., Kuster, W. C., and de Gouw, J. A.: Source signature of volatile organic compounds from oil and natural gas operations in Northeastern Colorado, Environ. Sci. Tech., 47, 1297–1305, doi:10.1021/es304119a, 2013.
Helmig, D., Bottenheim, J. Galbally, I. E., Lewis, A., Milton, M. J. T., Penkett, S., Plass-Duelmer, C., Reimann, S., Tans, P. P., Thiel, S.: Volatile organic compounds in the global atmosphere, Eos T. Am. Geophys. Un., 90, 513–514, doi:10.1029/2009EO520001, 2009.
Helmig, D., Thompson, C. R., Evans, J., Boylan, P., Hueber, J., and Park, J.-H.: Highly elevated levels of volatile organic compounds in the Uintah Basin, Utah, Environ. Sci. Technol., 48, 4707–4715, doi:10.1021/es405046r, 2014.
Karion, A., Sweeney, C., Wolter, S., Newberger, T., Chen, H., Andrews, A., Kofler, J., Neff, D., and Tans, P.: Long-term greenhouse gas measurements from aircraft, Atmos. Meas. Tech., 6, 511–526, doi:10.5194/amt-6-511-2013, 2013a.
Karion, A., Sweeney, C., Petron, G., Frost, G., Hardesty, R. M., Kofler, J., Miller, B. R., Newberger, T., Wolter, S., Banta, R., Brewer, A., Dlugokencky, E., Lang, P., Montzka, S. A., Schnell, R., Tans, P., Trainer, M., Zamora, R., and Conley, S.: Methane emissions estimate from airborne measurements over a western United States natural gas field, Geophys. Res. Lett., 40, 4393–4397, doi:10.1002/grl.50811, 2013b.

ACPD
14, 20117–20157, 2014

Lareau, N. P., Crosman, E., Whiteman, C. D., Horel, J. D., Hoch, S. W., Brown, W. O. J., and Horst, T. W.: The persistent cold-air pool study, B. Am. Meteorol. Soc., 94, 51–63, doi:10.1175/BAMS-D-11-00255.1, 2012.

Lyman, S. and Shorthill, H.: Final Report: 2012 Uintah Basin Winter Ozone & Air Quality Study. Doc. No. CRD13-320.32, Commercialization and Regional Development, Utah State University, available at: http://rd.usu.edu/files/uploads/ubos_2011-12_final_report.pdf (last access: 1 February), 2013.

Martin, R., K. Moore, Mansfield, M., Hill, S., Harper, K., and Shorthill, H.: Final Report: Uinta Basin Winter Ozone and Air Quality Study, December 2010 – March 2011, EDL/11-039, Energy Dynamics Lab., Utah State University Research Foundation, Bingham Research Center, Vernal, Utah, 14 June, 2011.

Miller, J. B., Lehman, S. J., Montzka, S. A., Sweeney, C., Miller, B. R., Karion, A., Wolak, C., Dlugokencky, E. J., Southon, J., Turnbull, J. C., and Tans, P. P.: Linking emissions of fossil fuel CO2 and other anthropogenic trace gases using atmospheric (CO_2)-C-14, J. Geophys. Res.-Atmos., 117, D08302, doi:10.1029/2011JD017048, 2012.

Neemann, E. M., Crosman, E. T., Horel, J. D., and Avey, L.: Simulations of a cold-air pool associated with elevated wintertime ozone in the Uintah Basin, Utah, Atmos. Chem. Phys. Discuss., 14, 15953–16000, doi:10.5194/acpd-14-15953-2014, 2014.

Oltmans, S., Schnell, R., Johnson, B., Pétron, G., Mefford, T., and Neely III, R.: Anatomy of wintertime ozone production associated with oil and gas extraction activity in Wyoming and Utah, Elem. Sci. Anth., 2, 000024, doi:10.12952/journal.elementa.000024, 2014.

Peischl, J., Ryerson, T. B., Holloway, J. S., Trainer, M., Andrews, A. E., Atlas, E. L., Blake, D. R., Daube, B. C., Dlugokencky, E. J., Fischer, M. L., Goldstein, A. H., Guha, A., Karl, T., Kofler, J., Kosciuch, E., Misztal, P. K., Perring, A. E., Pollack, I. B., Santoni, G. W., Schwarz, J. P., Spackman, J. R., Wofsy, S. C., and Parrish, D. D.: Quantifying sources of methane using light alkanes in the Los Angeles basin, California, J. Geophys. Res.-Atmos, 118, 4974–4990, doi:10.1002/jgrd.50413, 2013.

Pétron, G., Frost, G., Miller, B. R., Hirsch, A. I., Montzka, S. A., Karion, A., Trainer, M., Sweeney, C., Andrews, A. E., Miller, L., Kofler, J., Bar-Ilan, A., Dlugokencky, E. J., Patrick, L., Moore, C. T., Ryerson, T. B., Siso, C., Kolodzey, W., Lang, P. M., Conway, T., Novelli, P., Masarie, K., Hall, B., Guenther, D., Kitzis, D., Miller, J., Welsh, D., Wolfe, D., Neff, W., and Tans, P.: Hydrocarbon emissions characterization in the Colorado Front Range: a pilot study, J. Geophys. Res., 117, D04304, doi:10.1029/2011JD016360, 2012.

ACPD
14, 20117–20157, 2014

Rappenglück, B., Ackermann, L., Alvarez, S., Golovko, J., Buhr, M., Field, R. A., Soltis, J., Montague, D. C., Adamson, S, Risch, D., Wilkerson, G., Bush, D., Stoeckenius, T., and Kessler, C.: Strong wintertime ozone events in the Upper Green River, Wyoming, Atmos. Chem. Phys., 14, 4909–4934, doi:10.5194/acp-14-4909-2014, 2014

Schnell, R. C., Oltmans, S. J., Neely, R. R., Endres, M. S., Molenar, J. V., and White, A. B.: Rapid photochemical production of ozone at high concentrations in a rural site during winter, Nat. Geosci., 2, 120–122, doi:10.1038/ngeo415, 2009.

Schnell, R. C., Johnson, B., Cullis, P., Sterling, C., Hall, E., Albee, R., Jordan, A., Wendell, J., Oltmans, S., Petron, G., and Sweeney, C.: Ozone profiles from tethered ozonesondes in the Uintah Basin during UBWOS 2013, Atmos. Chem. Phys. Discuss., in preparation, 2014.

Stoeckenius, T. and McNally, D. (Eds.): Final Report 2013 Unita Basin Winter Ozone Study, available at: http://www.deq.utah.gov/locations/U/uintahbasin/studies/UBOS-2013.htm (last access: 23 July 2014), 2014.

Turnbull, J. C., Karion, A., Fischer, M. L., Faloona, I., Guilderson, T., Lehman, S. J., Miller, B. R., Miller, J. B., Montzka, S., Sherwood, T., Saripalli, S., Sweeney, C., and Tans, P. P.: Assessment of fossil fuel carbon dioxide and other anthropogenic trace gas emissions from airborne measurements over Sacramento, California in spring 2009, Atmos. Chem. Phys., 11, 705–721, doi:10.5194/acp-11-705-2011, 2011.

Warneke, C., Geiger, F., Edwards, P. M., Dube, W., Pétron, G., Kofler, J., Zahn, A., Brown, S. S., Graus, M., Gilman, J., Lerner, B., Peischl, J., Ryerson, T. B., de Gouw, J. A., and Roberts, J. M.: Volatile organic compound emissions from the oil and natural gas industry in the Uinta Basin, Utah: point sources compared to ambient air composition, Atmos. Chem. Phys. Discuss., 14, 11895–11927, doi:10.5194/acpd-14-11895-2014, 2014.

Wunch, D., Wennberg, P. O., Toon, G. C., Keppel-Aleks, G., and Yavin. Y. G.: Emissions of greenhouse gases from a North American megacity, Geophys. Res. Lett., 36, L15810, doi:10.1029/2009GL039825, 2009.

Yu, C.-H. and Pielke, R. A.: Mesoscale air quality under stagnant synoptic cold season conditions in the Lake Powell area, Atmos. Environ., 20, 1751–1762, 1986.

ACPD
14, 20117–20157, 2014

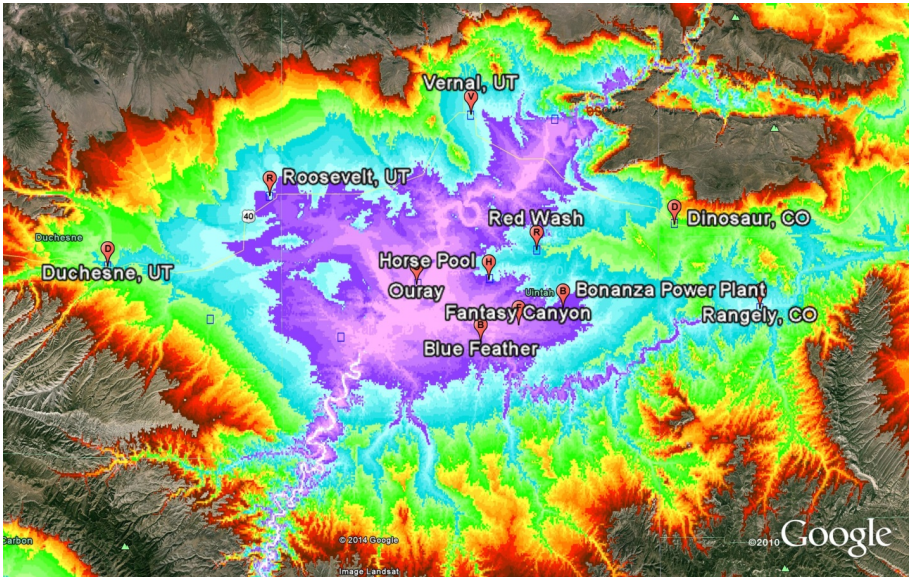

Figure 1. Topography of the Uinta Basin. The locations of surface measurement sites and several towns in the basin are also shown.

ACPD
14, 20117–20157, 2014

Figure 2. Photograph of the Cessna 210 aircraft that sampled over the Uinta Basin in February 2013. Three inlets and two temperature and humidity probes were installed under the starboard wing.

ACPD
14, 20117–20157, 2014

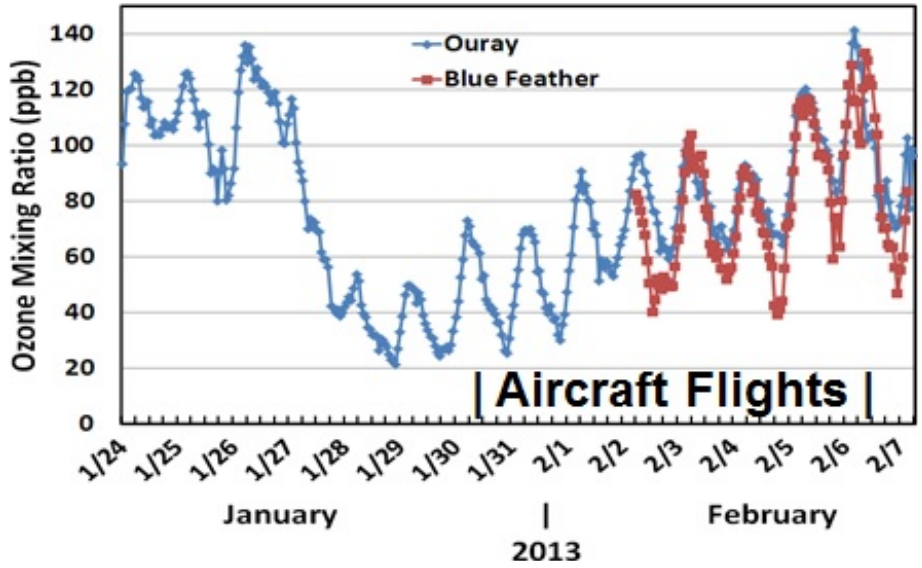

Figure 3. Hourly surface ozone (mole fractions) mixing ratios at two sites in the Uinta Basin (shown in Fig. 1) during January and February 2013 during the period of the aircraft flights showing the ozone buildup.

ACPD
14, 20117–20157, 2014

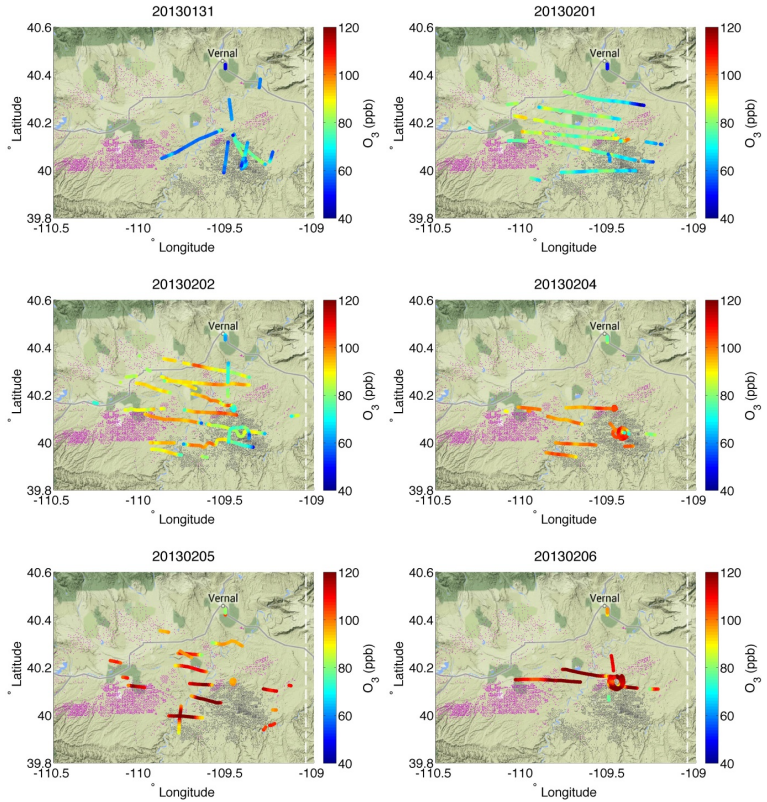

Figure 4. Map of flight tracks on 31 January, 1, 2, 4, 5, and 6 February 2013 over the Uinta Basin colored by mole fraction in parts per million (ppb) for O_3. The flight tracks show portions below 1650 m a.s.l. only. Locations of oil and gas wells are shown as magenta and gray dots, respectively. The flight date is indicated above each panel (YYYYMMDD).

ACPD
14, 20117–20157, 2014

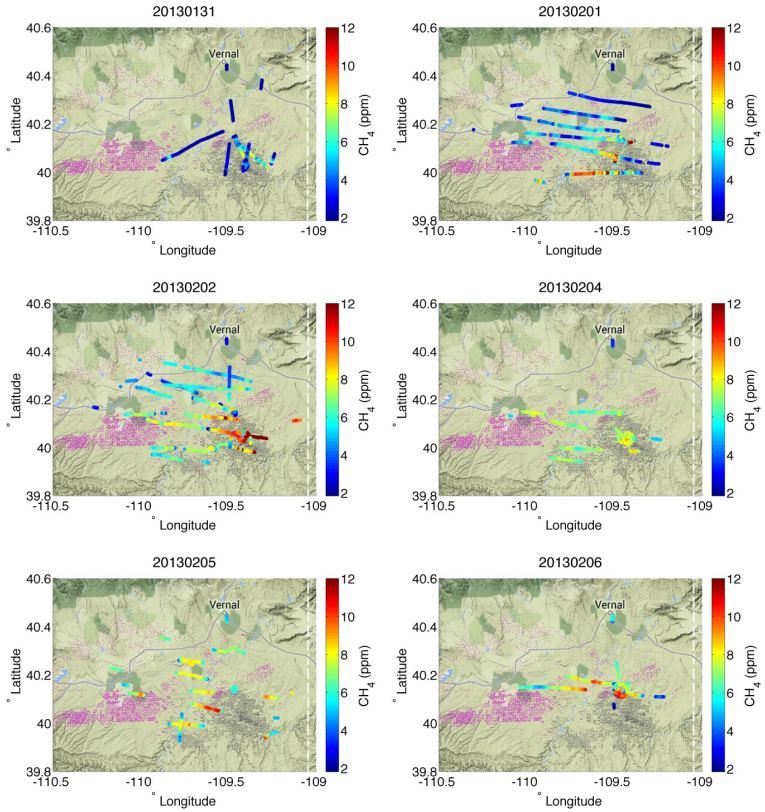

Figure 5. Map of flight tracks for CH_4 on 31 January, 1, 2, 4, 5, and 6 February 2013 over the Uinta Basin colored by mole fraction in parts per million (ppm). The flight tracks are for portions below 1650 m a.s.l. only. Locations of oil and gas wells are shown as magenta and gray dots, respectively. The flight date is indicated above each panel (YYYYMMDD).

ACPD
14, 20117–20157, 2014

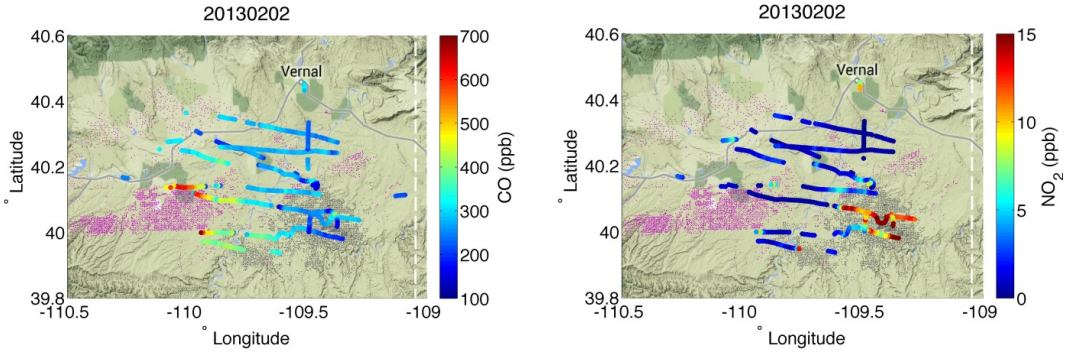

Figure 6. Map of flight tracks for CO and NO_2 on 2 February 2013 over the Uintah Basin colored by mole fraction in parts per million (ppb). The flight tracks are for portions below 1650 m a.s.l. only. Locations of oil and gas wells are shown as purple and gray dots, respectively. The flight date is indicated above each panel (YYYYMMDD).

ACPD
14, 20117–20157, 2014

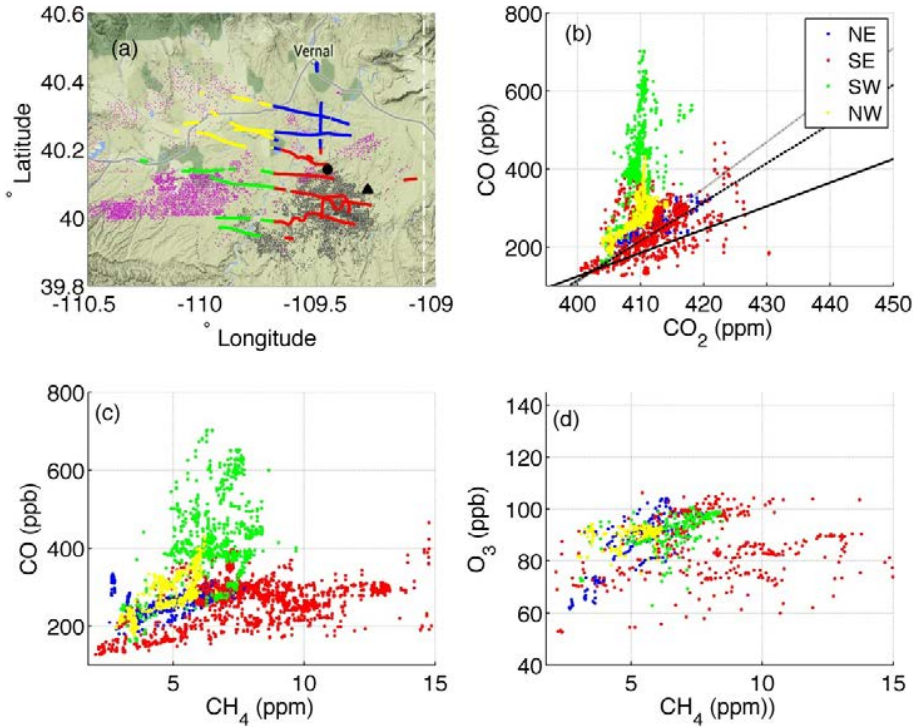

Figure 7. Spatial analysis of trace gas dry air mole fraction correlations during the 2 February 2013 flight. **(a)** Map of the flight track below the inversion (1650 m a.s.l.) colored by quadrant (red: SE, blue: NE, yellow: NW, green: SW). The location of Horse Pool is noted with a black circle; the Bonanza power plant is a black triangle. **(b)** Correlation plot of CO with CO_2 in the four quadrants. Black dotted line shows a molar ratio of 12 ppb CO per ppm of CO_2, dashed line is 10 ppb ppm^{-1}, and solid line is 6 ppb ppm^{-1}. **(c)** Correlation plot of CO with CH_4, indicating more CO emission per unit CH_4 in the SW quadrant, and more CH_4 per unit CO in the SE. **(d)** Correlations of CH_4 with O_3 mole fractions show less spatial separation, supporting the observation that O_3 is observed more uniformly through the region.

ACPD
14, 20117–20157, 2014

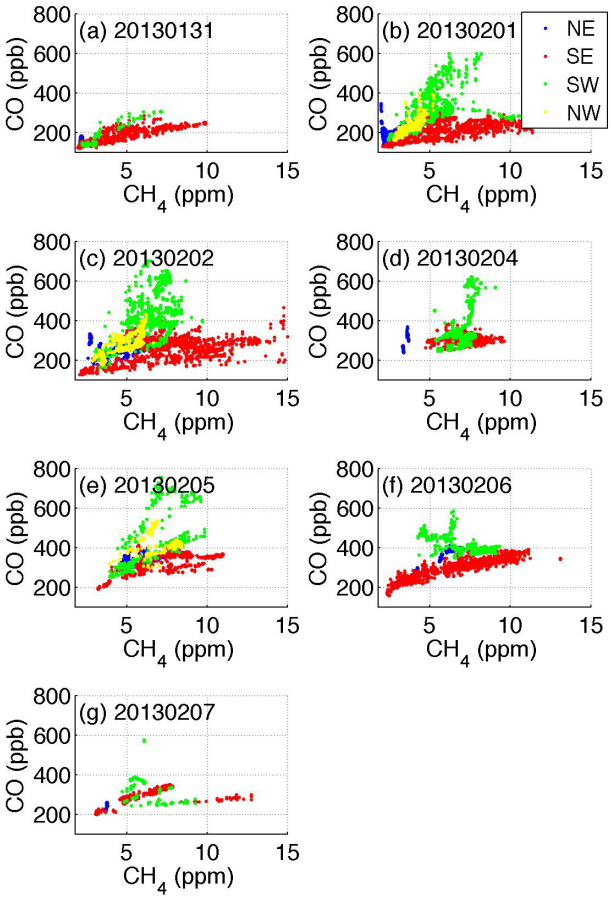

Figure 8. Relationship between CO with CH_4 over the different quadrants of the basin for the seven flights with the flight date indicated in each panel (YYYYMMDD).

ACPD
14, 20117–20157, 2014

A high ozone episode in winter 2013 in the Uinta Basin oil and gas region

S. J. Oltmans et al.

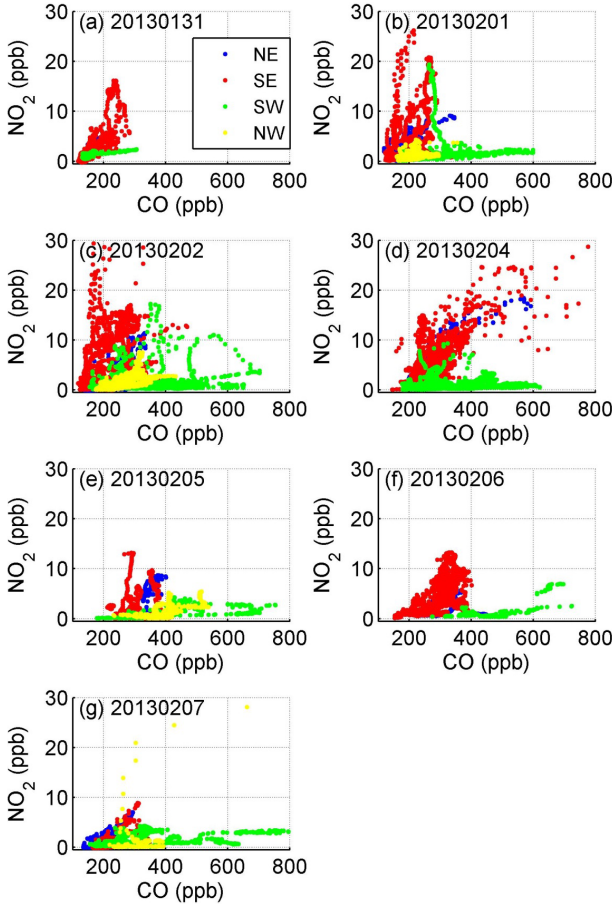

Figure 9. Relationship between NO_2 with CO over the different quadrants of the basin for the seven flights with the flight date indicated in each panel (YYYYMMDD).

ACPD
14, 20117–20157, 2014

A high ozone episode in winter 2013 in the Uinta Basin oil and gas region

S. J. Oltmans et al.

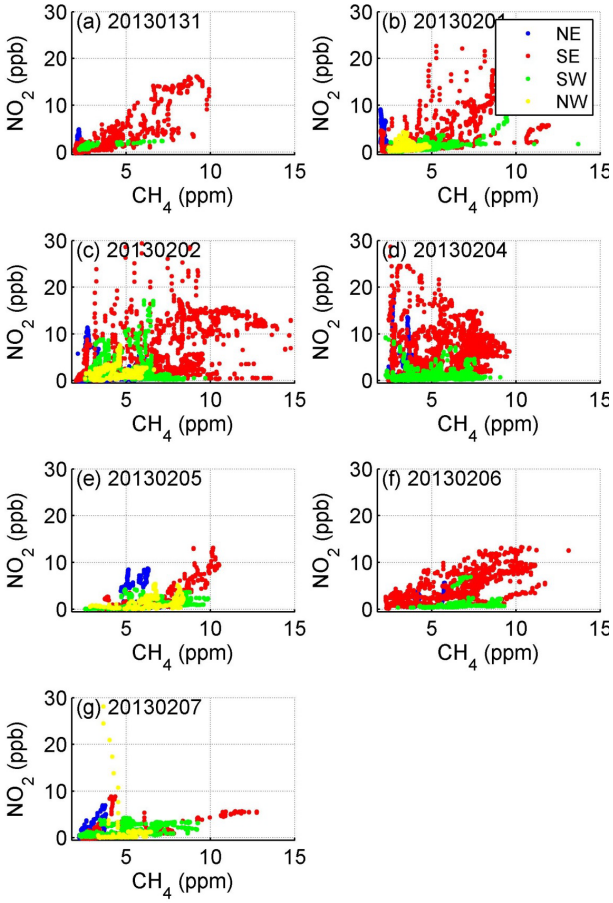

Figure 10. Relationship between NO_2 and CH_4 over the different quadrants of the basin for the seven flights with the flight date indicated in each panel (YYYYMMDD).

ACPD
14, 20117–20157, 2014

A high ozone episode in winter 2013 in the Uinta Basin oil and gas region

S. J. Oltmans et al.

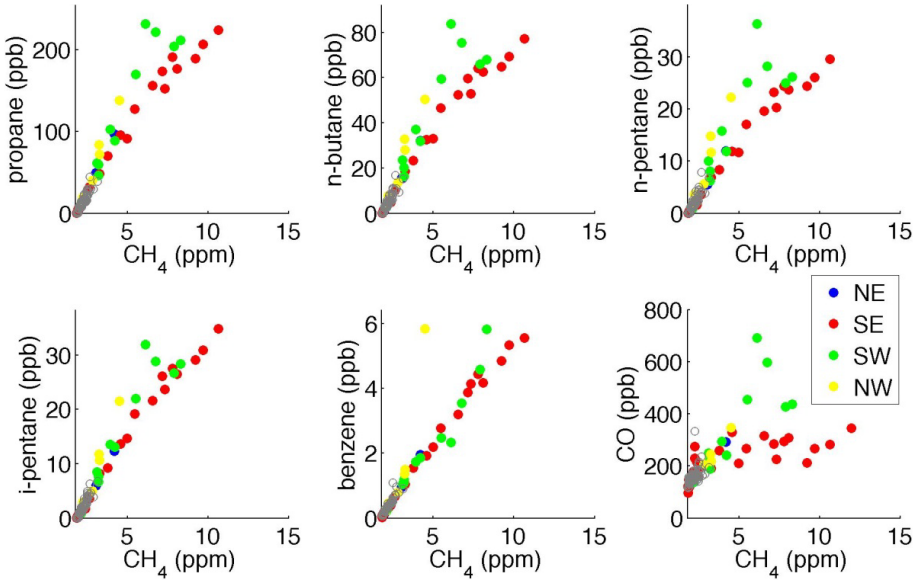

Figure 11. Measurements of light hydrocarbons (first five panels) and CO (bottom right) plotted against CH_4 mole fraction from air samples collected in flasks over the Uinta Basin in 2013 (blue, red, green or yellow based on quadrant) and 2012 (gray).

ACPD
14, 20117–20157, 2014

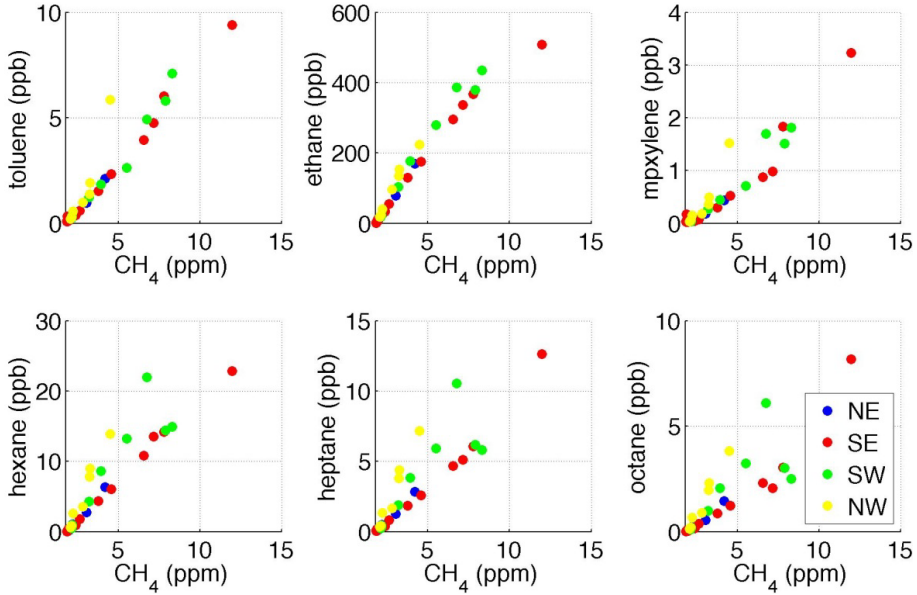

Figure 12. Measurements of heavier hydrocarbons in flasks collected aboard the aircraft, 31 January–7 February 2013, colored by quadrant.

ACPD
14, 20117–20157, 2014

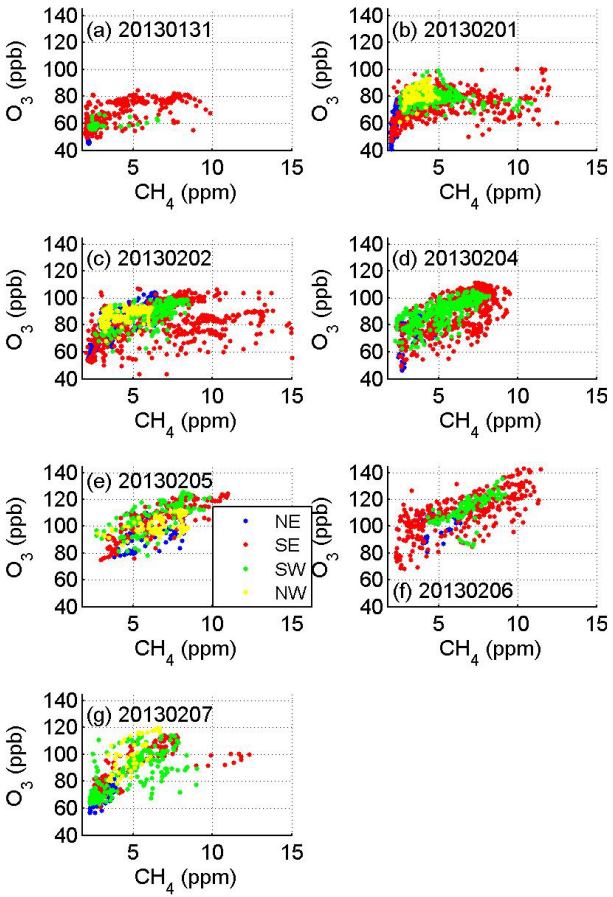

Figure 13. Relationship between O_3 and CH_4 over the different quadrants of the basin for the seven flights with the flight date indicated in each panel (YYYYMMDD).

ACPD
14, 20117–20157, 2014

A high ozone episode in winter 2013 in the Uinta Basin oil and gas region

S. J. Oltmans et al.

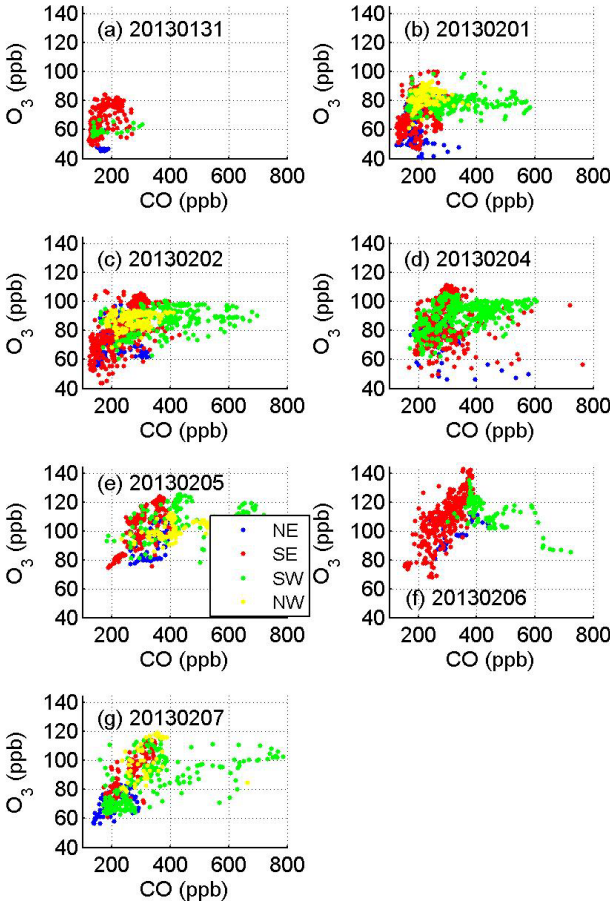

Figure 14. Relationship between O_3 and CO over the different quadrants of the basin for the seven flights with the flight date indicated in each panel (YYYYMMDD).

ACPD
14, 20117–20157, 2014

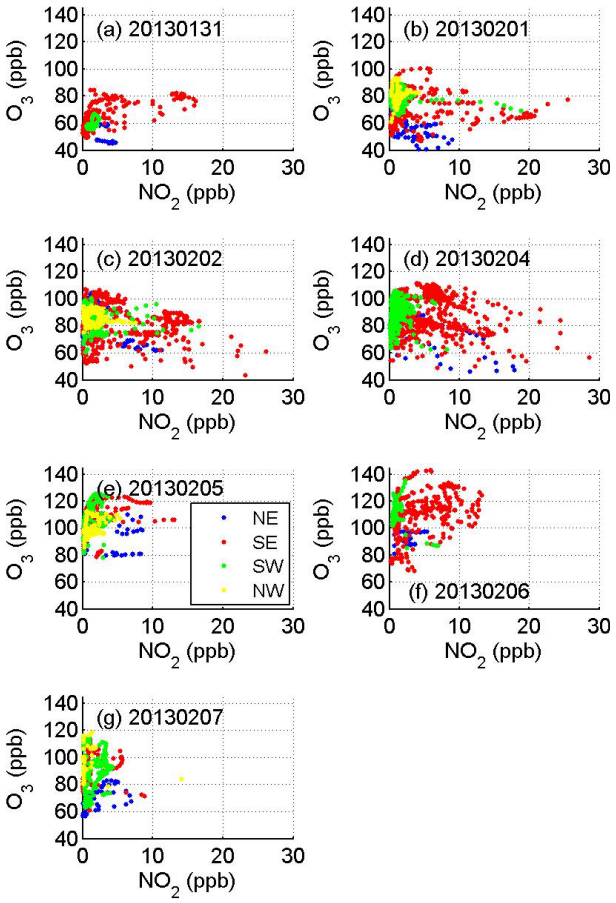

Figure 15. Relationship between O_3 and NO_2 over the different quadrants of the basin for the seven flights with the flight date indicated in each panel (YYYYMMDD).

ACPD
14, 20117–20157, 2014

A high ozone episode in winter 2013 in the Uinta Basin oil and gas region

S. J. Oltmans et al.

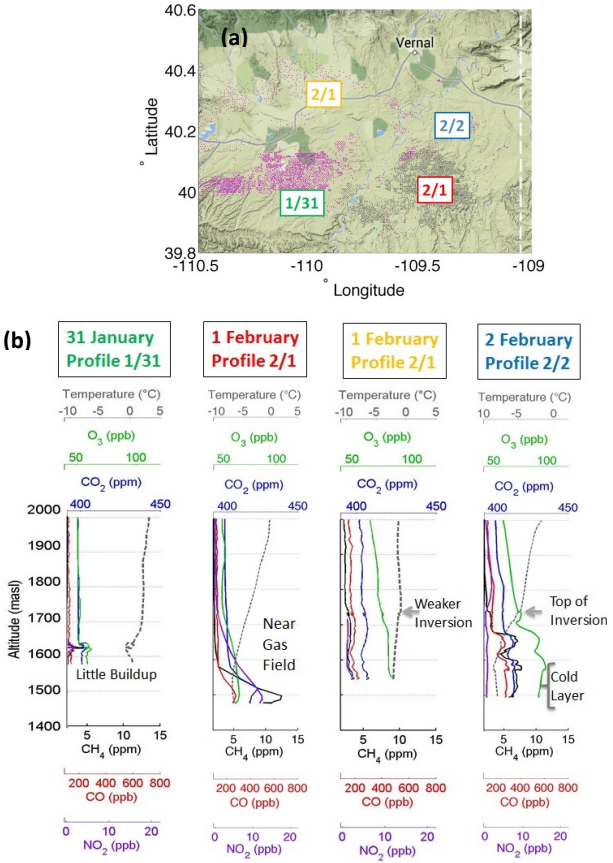

Figure 16. (a) Locations of the profiles in the Uinta Basin obtained on 31 January (1/31), 1 February (2/1 – 2 profiles) and 2 February (2/2), shown along with the oil (magenta) and gas (gray) well locations. **(b)** Four vertical profiles of CH_4 (black), CO (red), CO_2 (blue), O_3 (green) and NO_2 (purple) on 31 January, 1 February (2 profiles), and 2 February 2013.

ACPD
14, 20117–20157, 2014

A high ozone episode in winter 2013 in the Uinta Basin oil and gas region

S. J. Oltmans et al.

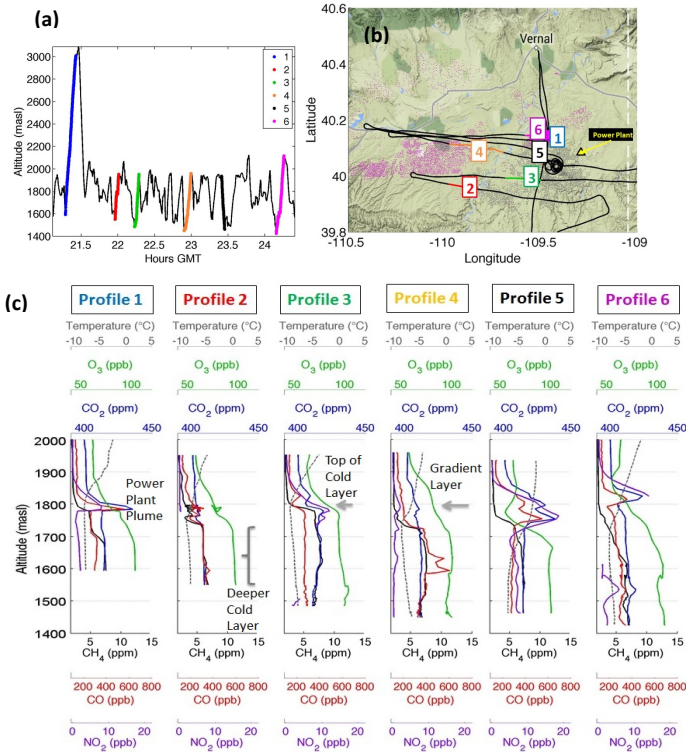

Figure 17. (a) Time series of flight on 4 February 2013, with the profiles highlighted. Local Standard Time is GMT-7 h. **(b)** Corresponding locations of the profiles in the Uinta Basin, shown along with the oil (magenta) and gas (gray) well locations. The Bonanza Power Plant is located at the black triangle. **(c)** Six vertical profiles of CH_4 (black), CO (red), CO_2 (blue), O_3 (green) and NO_2 (purple) from the flight on 4 February 2013. Temperature is shown in a dashed gray line (top axis).

ACPD
14, 20117–20157, 2014

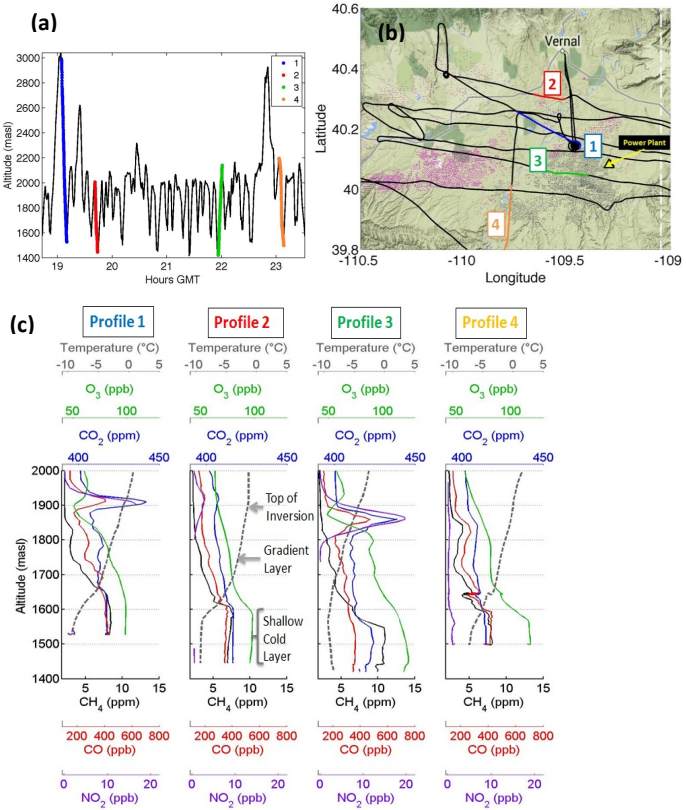

Figure 18. (a) Time series of flight on 5 February 2013, with the profiles highlighted. Local Standard Time is GMT-7 h. **(b)** Corresponding locations of the profiles in the Uinta Basin, shown along with the oil (magenta) and gas (gray) well locations. The Bonanza Power Plant is located at the black triangle. **(c)** Four vertical profiles of CH_4 (black), CO (red), CO_2 (blue), O_3 (green) and NO_2 (purple) from the flight on 5 February 2013. Temperature is shown in a dashed gray line (top axis).

ACPD
14, 20117–20157, 2014

A high ozone episode in winter 2013 in the Uinta Basin oil and gas region

S. J. Oltmans et al.

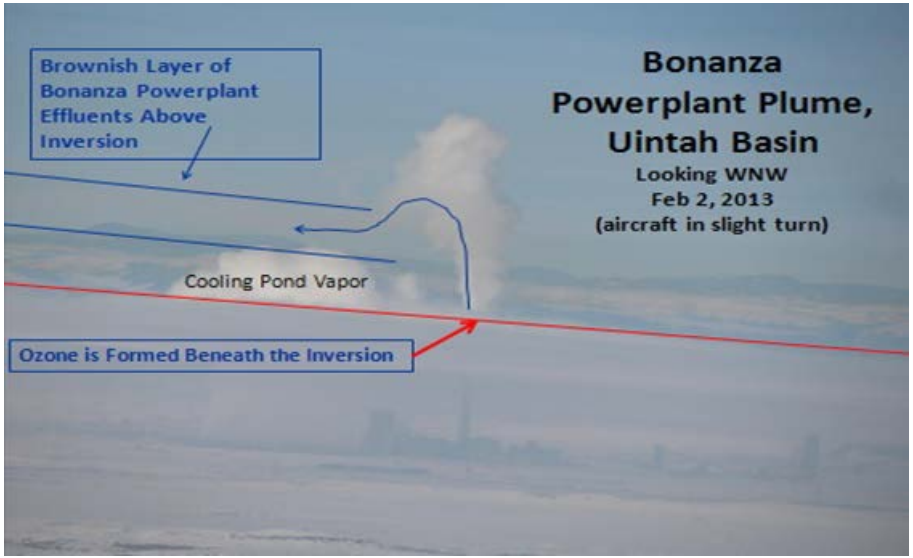

Figure 19. Photograph taken from the aircraft of the Bonanza Power Plant and its plume rising above the inversion layer defined by the haze below the inversion.

ACPD
14, 20117–20157, 2014

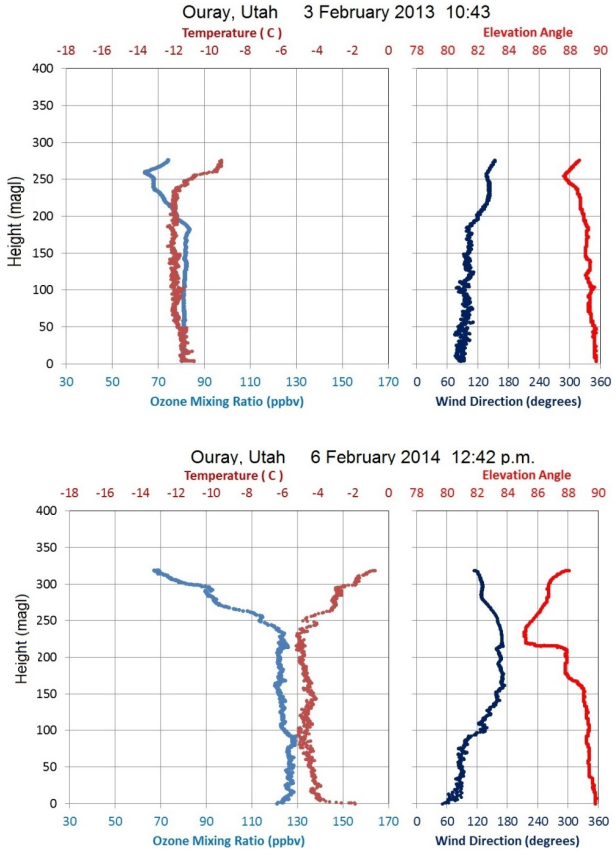

Figure 20. Tethered ozonesonde profiles on 3 and 6 February at Ouray. The left panel for each sounding shows O_3 (blue) and T (red). The right panel shows elevation angle (red) of the balloon from which the wind direction (dark blue) is derived.

ACPD
14, 20117–20157, 2014